Supplementary Information

Balancing Charge Transport and C–N Bond Strength in Stability-Oriented Host Design for Blue TADF-OLEDs

Domantas Berenis,[a] Giedrius Puidokas,[a] Kristupas Bagdonas,[a] Goda Grybauskaitė,[a] Dovydas Banevičius,[a] Gediminas Kreiza,[a] Eigirdas Skuodis,[a] Rita Butkutė,[b] Juozas V. Gražulevičius [b] and Karolis Kazlauskas *[a]

E-mail: karolis.kazlauskas@ff.vu.lt

Institute of Photonics and Nanotechnology, Vilnius University, Saulėtekio av. 3, LT-10257 Vilnius, Lithuania

Department of Polymer Chemistry and Technology, Faculty of Chemical Technology, Kaunas University of Technology, Baršausko 59, LT-51423, Kaunas, Lithuania

Synthesis

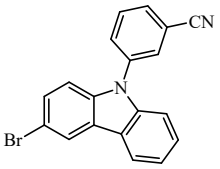

3-(3-bromo-9H-carbazol-9-yl)benzonitrile. Mixture of 3-bromo-9*H*-carbazole (2 g, 8.14 mmol), *t*-BuONa (1.56 g, 16.26 mmol) and catalytic amount of 15-crown-5 was diluted in 40 ml of DMF and stirred for 30 minutes at room temperature. After addition of 3-fluorobenzonitrile (1.46 g, 12.20 mmol) reaction mixture was stirred at 50 °C overnight. After cooling to room temperature, the mixture was poured into water and extracted with ethylacetate. The organic extracts were collected and dried with anhydrous Na_2SO_4. After removal of the solvent, the residue was purified by crystallization from methanol to obtain pale yellow solid. Yield: 88%.

^{1}H NMR (400 MHz, $CDCl_3$, δ) 8.14 (s, 1H), 7.98 (d, *J* = 7.8 Hz, 1H), 7.77 – 7.60 (m, 4H), 7.38 (dd, *J* = 19.7, 8.3 Hz, 2H), 7.29 – 7.20 (m, 2H), 7.13 (d, *J* = 8.7 Hz, 1H).

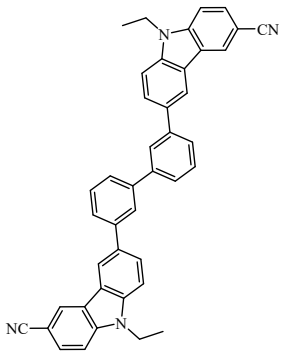

6,6'-([1,1'-biphenyl]-3,3'-diyl)bis(9-ethyl-9H-carbazole-3-carbonitrile) (**mCzB-2CN**). THF (10 mL) and degassed water (5 ml) was added to a mixture of 6-bromo-9-ethyl-9H-carbazole-3-carbonitrile (0.68 g, 2.27 mmol), 3,3'-bis(4,4,5,5-tetramethyl-1,3,2-dioxaborolan-2-yl)-1,1'-biphenyl (0.40 g, 1.00 mmol), K_2CO_3 (0.63 g, 5.0 mmol), and $PdCl_2(PPh_3)_2$ (0.04 g, 0.06 mmol). The mixture was refluxed for 2 h under argon. After cooling to room temperature, the mixture was poured into water and extracted with ethyl acetate. The organic extract was collected and dried with anhydrous Na_2SO_4. After removal of the solvent, the residue was purified by column chromatography on silica gel using ethyl acetate/hexane (1 : 6 v/v) for the eluent to give **mCzB-2CN** as a white powder. Yield: 71%.

^{1}H NMR (400 MHz, $CDCl_3$, δ) 8.45 (s, 2H), 8.39 (s, 2H), 8.00 (s, 2H), 7.88 (d, *J* = 8.3 Hz, 2H), 7.75 – 7.65 (m, 6H), 7.66 – 7.59 (m, 2H), 7.56 (d, *J* = 8.6 Hz, 2H), 7.46 (d, *J* = 8.6 Hz, 2H), 4.43 (q, *J* = 6.9 Hz, 4H), 1.49 (t, *J* = 7.0 Hz, 6H). **^{13}C NMR** (101 MHz, $CDCl_3$, δ) 142.22, 142.17, 142.11, 140.18, 134.00, 129.56, 129.29, 126.92, 126.61, 126.56, 126.06, 125.57, 123.34, 122.74, 120.70, 119.54, 109.42, 101.83, 38.19, 13.99. **MS-ESI$^+$:** m/z calcd. for $C_{42}H_{30}N_4$: 590.25; found: 590.46.

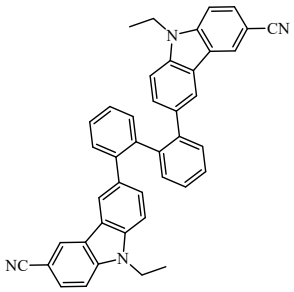

6,6'-([1,1'-biphenyl]-2,2'-diyl)bis(9-ethyl-9H-carbazole-3-carbonitrile) (**oCzB-2CN**). THF (11 mL) and degassed water (5.5 ml) was added to a mixture of 6-bromo-9-ethyl-9H-carbazole-3-carbonitrile (0.97 g, 3.30 mmol), 2,2'-bis(4,4,5,5-tetramethyl-1,3,2-dioxaborolan-2-yl)-1,1'-biphenyl (0.60 g, 1.50 mmol), K_2CO_3 (0.96 g, 7.5 mmol), and $PdCl_2(PPh_3)_2$ (0.06 g, 0.09 mmol). The mixture was refluxed for 4 h under argon. After cooling to room temperature, the

mixture was poured into water and extracted with ethylacetate. The organic phase was collected and dried with anhydrous Na_2SO_4. After removal of the solvent, the residue was purified by column chromatography on silica gel using ethylacetate/hexane (1 : 10 v/v) for the eluent to give **oCzB-2CN** as a white powder. Yield: 57%.

^{1}H NMR (400 MHz, $CDCl_3$, δ) 7.66 (d, *J* = 7.5 Hz, 2H), 7.52 (t, *J* = 7.3 Hz, 2H), 7.43 (d, *J* = 8.1 Hz, 4H), 7.33 (d, *J* = 8.4 Hz, 2H), 7.15 (d, *J* = 8.1 Hz, 4H), 6.99 (d, *J* = 8.6 Hz, 2H), 6.75 (d, *J* = 8.3 Hz, 2H), 6.57 (s, 2H), 4.34 (q, *J* = 7.0 Hz, 4H), 1.51 (t, *J* = 7.0 Hz, 6H). **^{13}C NMR** (101 MHz, $CDCl_3$, δ) 141.40, 141.07, 140.34, 138.77, 133.84, 132.04, 130.18, 128.66, 128.18, 127.99, 127.52, 123.40, 122.69, 121.98, 120.73, 108.94, 107.31, 101.11, 38.01, 14.15. **MS-ESI$^+$:** m/z calcd. for $C_{42}H_{30}N_4$: 590.25; found: 590.72.

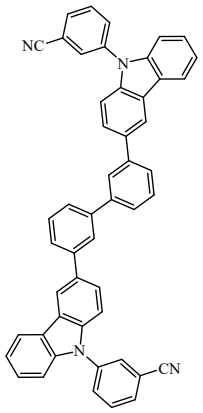

3,3'-([1,1'-biphenyl]-3,3'-diylbis(9H-carbazole-3,9-diyl))dibenzonitrile (**mCzB-2PhCN**). THF (10 mL) and degassed water (5 ml) was added to a mixture of 3-(3-bromo-9H-carbazol-9-yl)benzonitrile (2.22 g, 6.39 mmol), 3,3'-bis(4,4,5,5-tetramethyl-1,3,2-dioxaborolan-2-yl)-1,1'-biphenyl (1.00 g, 2.46 mmol), Cs_2CO_3 (4.80 g, 14.7 mmol), and $PdCl_2(PPh_3)_2$ (0.10 g, 0.14 mmol). The mixture was refluxed overnight under argon. After cooling to room temperature, the mixture was poured into water and extracted with ethyl acetate. The organic extract was collected and dried with anhydrous Na_2SO_4. After removal of the solvent, the residue was purified by column chromatography on silica gel using tetrahydrofuran/hexane (1 : 2 v/v) for the eluent to give **mCzB-2PhCN** as a white powder. Yield: 49%.

^{1}H NMR (400 MHz, $CDCl_3$, δ) 8.43 (s, 2H), 8.21 (d, *J* = 7.6 Hz, 2H), 8.03 (s, 2H), 7.96 – 7.84 (m, 4H), 7.80 – 7.67 (m, 10H), 7.65 – 7.58 (m, 2H), 7.51 – 7.43 (m, 4H), 7.41 (d, *J* = 7.9 Hz, 2H), 7.36 (t, *J* = 7.3 Hz, 2H). **^{13}C NMR** (101 MHz, $CDCl_3$, δ) 142.41, 142.14, 140.84, 139.93, 138.97, 134.41, 131.57, 131.20, 130.39, 129.50, 126.75, 126.62, 126.61, 126.08, 126.01,

124.50, 123.97, 121.13, 120.85, 119.35, 114.44, 109.77, 109.59. **MS-ESI$^+$:** m/z calcd. for $C_{50}H_{30}N_4$: 686.25; found: 685.72.

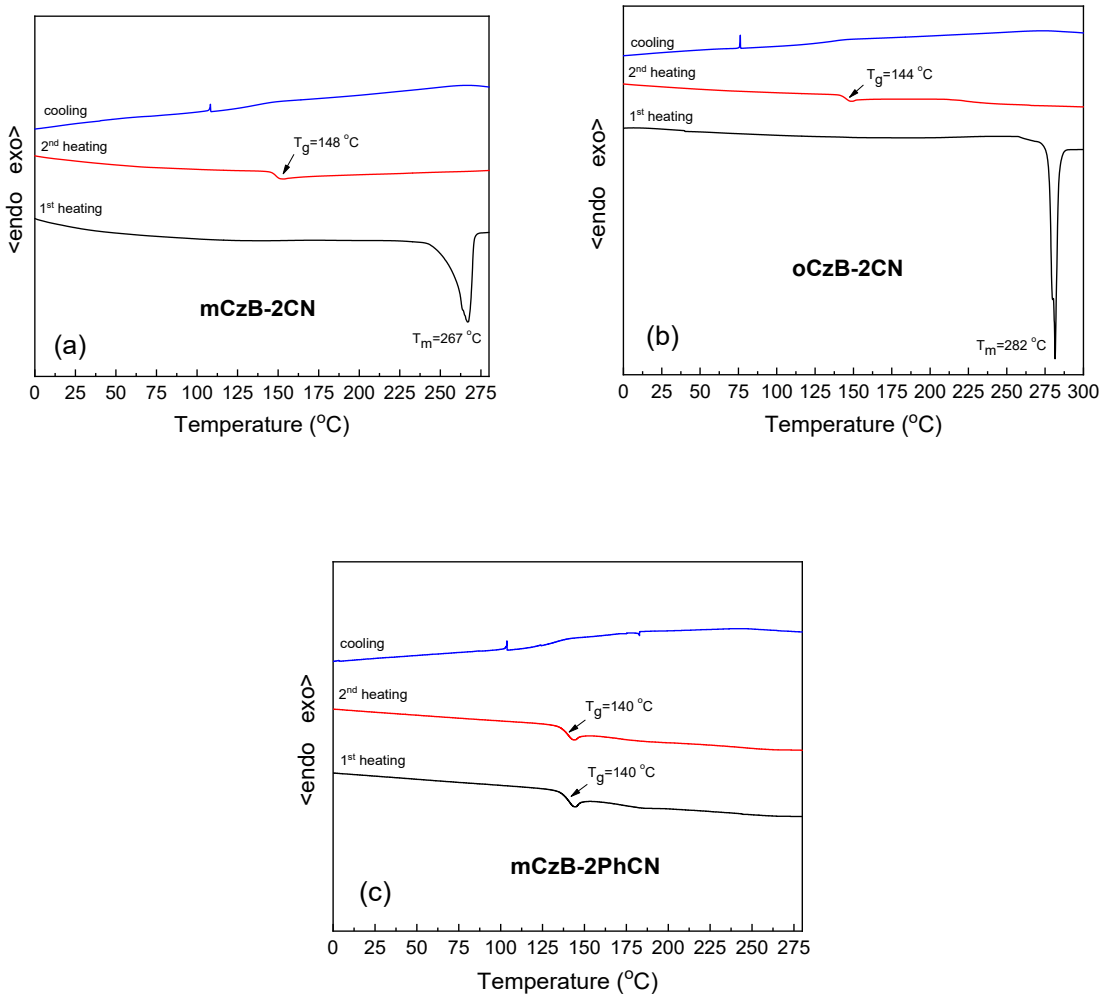

Figure S1. DSC heating-cooling scans of the carbazole–biphenyl hosts (a) **mCzB-2CN**, (b) **oCzB-2CN**, and (c) **mCzB-2PhCN** recorded under nitrogen atmosphere at a heating/cooling rate of 10 °C/min. Glass-transition (T_g) and melting transition (T_m) temperatures, indicated.

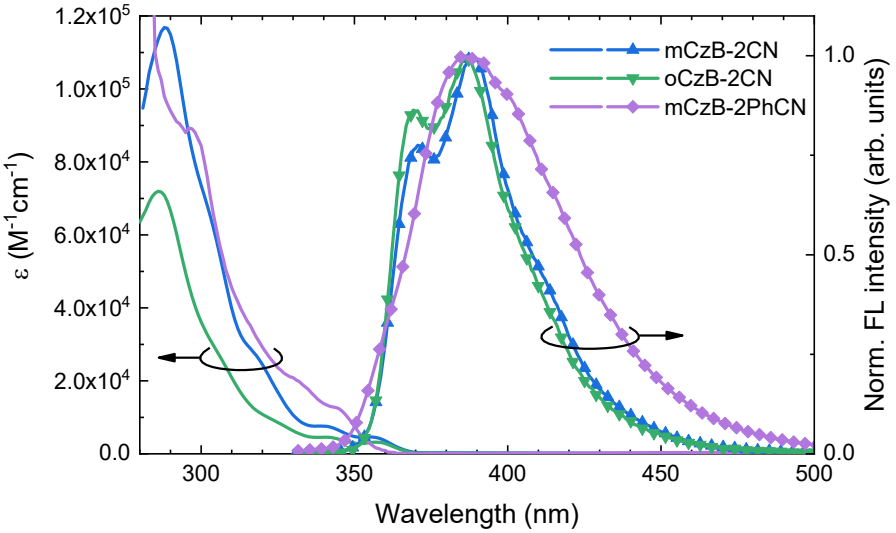

Figure S2. Absorption (line) and FL (line+symbol) spectra of **mCzB-2CN**, **oCzB-2CN**, and **mCzB-2PhCN** in toluene at 1×10^{-5} M concentration.

In dilute toluene solutions (Fig. S2), all three hosts display intense π–π* absorption bands in the UV (peaking at 290–310 nm, ε up to ~1×10^5 M^{-1} cm^{-1}) arising from the carbazole–biphenyl framework, with weak low-energy shoulders near 340–360 nm. The FL profiles feature a vibronically structured band in the near-UV/blue range, consistent with emission from the lowest singlet excited state. The zeroth vibronic bands of **mCzB-2CN** and **oCzB-2CN** peak at ~370 nm, while that of **mCzB-2PhCN** is slightly red-shifted (~385 nm) with broader tailing to ~480–500 nm.

The red shift follows the trend in LUMO localization inferred from DFT (**mCzB-2CN**/**oCzB-2CN** on carbazoles vs. **mCzB-2PhCN** on N-substituted cyano–phenyl groups), indicating increasing charge-transfer contribution in **mCzB-2PhCN**. Correspondingly, the apparent Stokes shift is smaller for **mCzB-2CN** and **oCzB-2CN** as compared to **mCzB-2PhCN**, reflecting stronger excited-state relaxation in the N-phenylated analogue. The spectral information implies that the position of the electron-accepting cyano moiety tunes the lowest-energy transition and emission energy while preserving strong UV absorption from the common carbazole–biphenyl core.

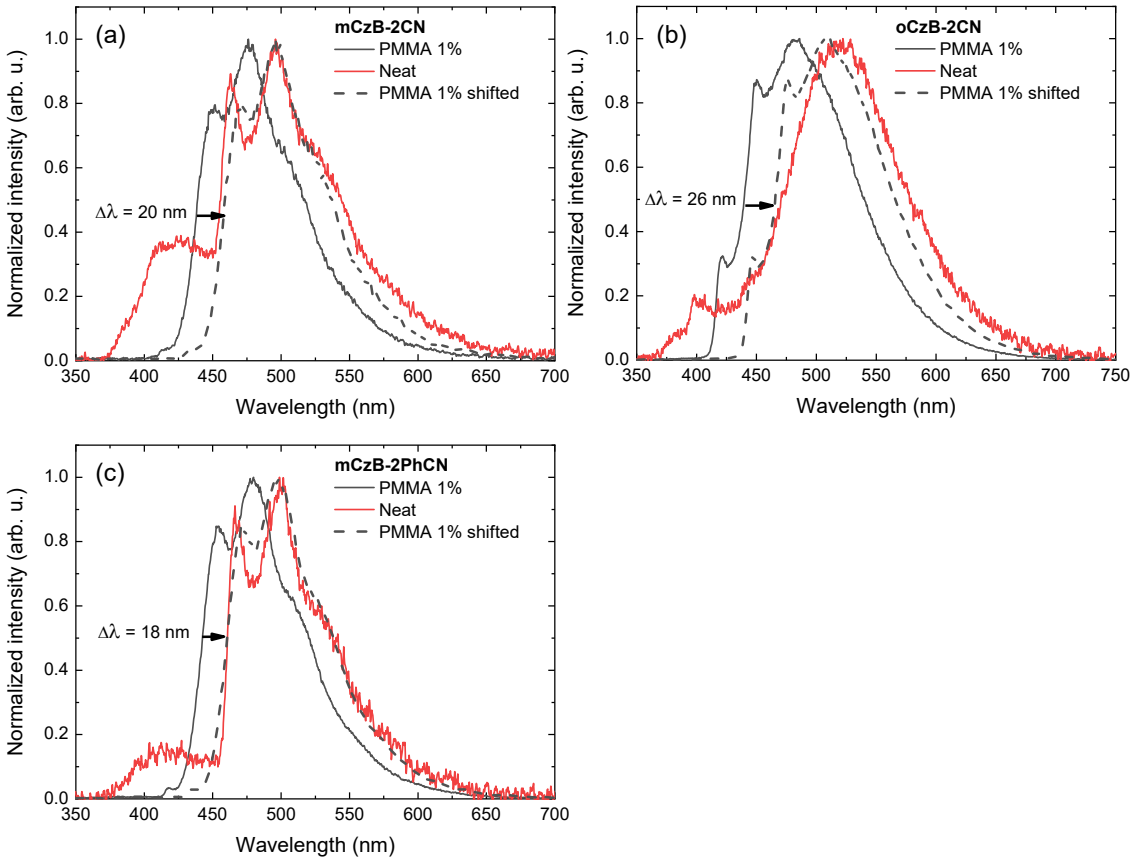

Figure S3. Estimation of the neat film T_1 energy by shifting 1 wt% PMMA film phosphorescence spectra to align with the neat film phosphorescence spectrum for (a) **mCzB-2CN**, (b) **oCzB-2CN**, and (c) **mCzB-2PhCN**. Overlaying phosphorescence spectra allows to eliminate delayed FL in the neat films emerging from TTA. T_1 of the neat film were calculated from the most energetic peak of the shifted 1 wt% PMMA film phosphorescence spectrum.

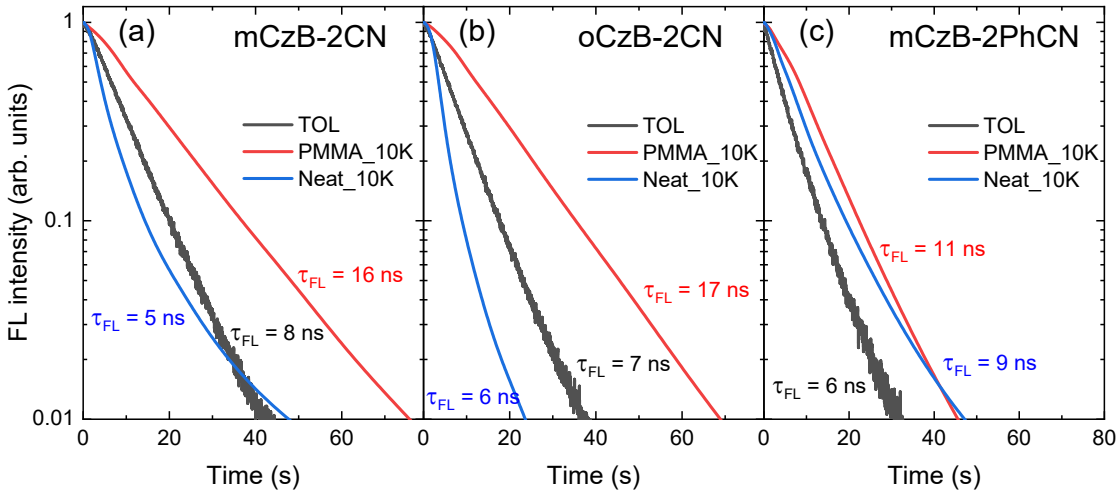

Figure S4. FL decay transients of (a) **mCzB-2CN**, (b) **oCzB-2CN**, and (c) **mCzB-2PhCN** in toluene (10^{-5}M, black), 1 wt% PMMA films (red), and neat films (blue). Traces were recorded at 10 K (solid state) and room temperature (solution). Average FL lifetimes, indicated.

FL transients in toluene revealed similar average lifetimes (τ_{FL}) for all three hosts, $\tau \approx 6 – 8$ ns (Fig. S4). In 1 wt% PMMA films measured at 10 K, the rigid matrix and low temperatures suppressed non-radiative decay, extending τ_{FL} to 11 – 16 ns. Neat films, by contrast, exhibited accelerated decays ($\tau_{FL} \approx 5 – 9$ ns) owing to intermolecular coupling, exciton migration, and concentration quenching. They show pronounced non-exponential FL decays because excitons undergo Förster-type hopping in a heterogeneous energy landscape and are quenched at traps/aggregates, yielding dispersive kinetics rather than a single-rate decay.[1] The smallest τ_{FL} shortening occurred for **mCzB-2PhCN** (11 → 9 ns), consistent with partial steric shielding by its peripheral cyano–phenyl groups.

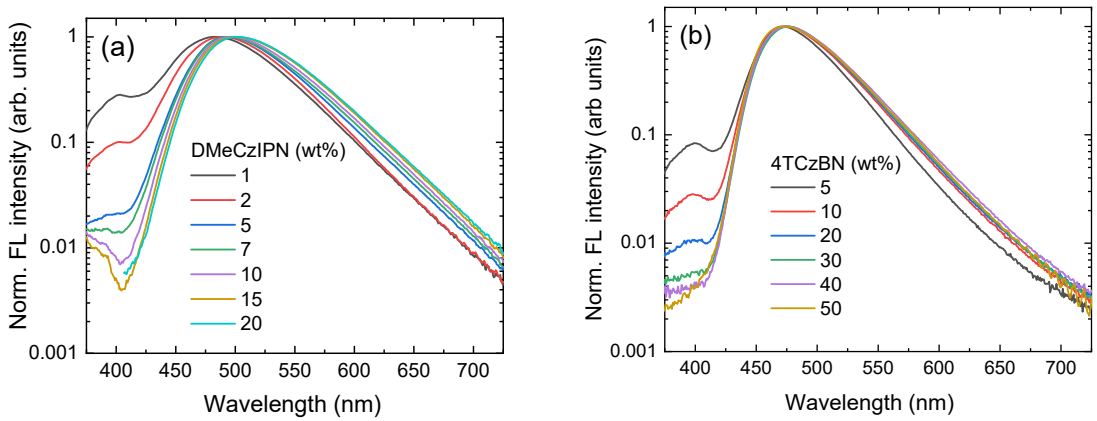

Figure S5. Normalized FL spectra of **mCzB-2CN** films doped with blue TADF emitters (a) DMeCzIPN and (b) 4TCzBN at various concentrations, indicated. Excitation wavelength, 350 nm.

Table S1. PLQY values of blue TADF emitters DMeCzIPN and 4TCzBN in **mCzB-2CN**, **oCzB-2CN**, and **mCzB-2PhCN** hosts at various doping concentrations.

	DMeCzIPN:Host x wt% (%)				**4TCzBN:Host x wt% (%)**		
Host	**7**	**10**	**15**	**20**	**30**	**40**	**50**
mCzB-2CN	43	45	49	52	47	50	52
oCzB-2CN	27	31	35	39	38	40	42
mCzB-2PhCN	44	50	51	52	54	57	55

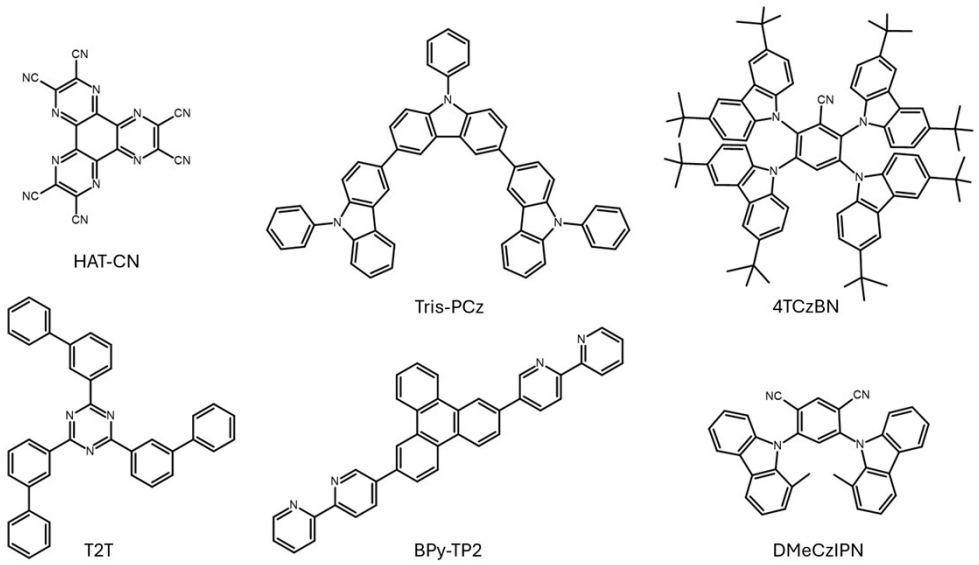

Figure S6. Chemical structures of HAT-CN, Tris-PCz, 4TCzBN, T2T, BPy-TP2 and DMeCzIPN used in OLED fabrication.

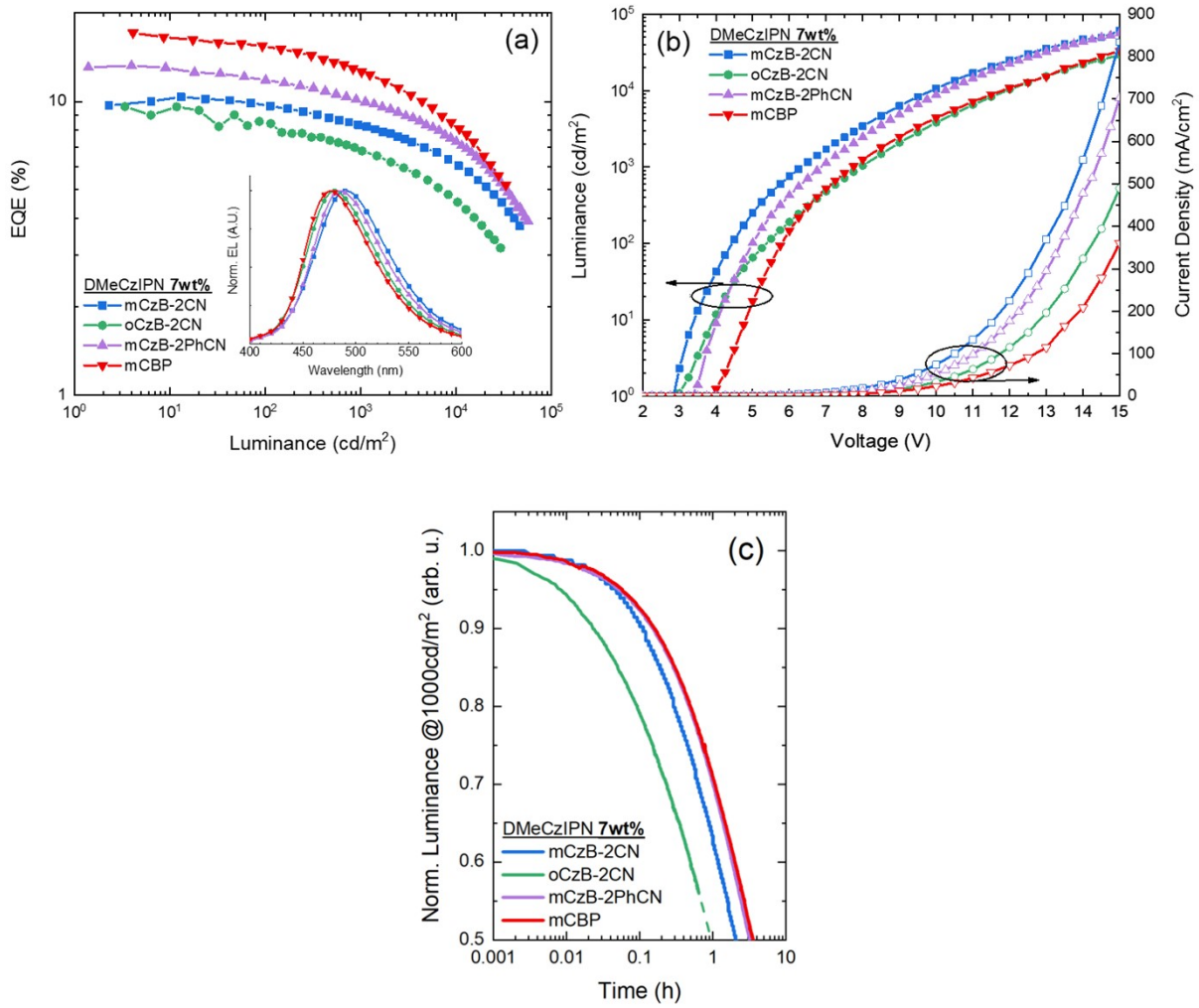

Figure S7. Performance comparison of blue TADF-OLEDs based on carbazole–biphenyl hosts (**mCzB-2CN**, **oCzB-2CN**, **mCzB-2PhCN**) and the commercial host mCBP using DMeCzIPN (7 wt%) as the emitter. (a) EQE vs. luminance (inset: normalized EL spectra). (b) J–V–L characteristics: luminance and current density vs. applied voltage. (c) Normalized luminance as a function of time measured under constant-current operation at an initial luminance of 1000 cd/m^2.

The mCBP device shows a higher EQE_{max} = 17.1% than our best host (**mCzB-2PhCN**) while exhibiting comparable operational stability (LT_{50} = 3.6 h at 1000 cd m^{-2}). This is not unexpected, since absolute EQE depends strongly on charge injection/transport balance in a given stack. Moreover, at fixed luminance a higher-EQE implies a lower operating current density, reducing polaron/exciton densities and therefore the probability of TPA-mediated degradation.

Table S2. Main electroluminescence parameters of blue TADF-OLEDs with varied EML compositions.

EML	V_{on} [a], V	$V_{@1000cd/m2}$, V	EQE_{max}, %	$EQE_{@1000cd/m2}$, %	λ_{EL} [b], nm	CIE, (x, y)	LT_{50} [c], h
mCzB-2CN:DMeCzIPN 7%	2.75	6.5	10.4	8.3	490	(0.18, 0.36)	2
oCzB-2CN:DMeCzIPN 7%	3	8	9.6	6.8	480	(0.17, 0.29)	0.95
mCzB-2PhCN:DMeCzIPN 7%	3.25	7	13.2	10.3	485	(0.18, 0.34)	3.2
mCBP:DMeCzIPN 7%	4	7.75	17.1	12.6	476	(0.16, 0.27)	3.6

[a] Turn-on voltage measured at 1 cd/m^2.
[b] EL peak wavelength
[c] Device lifetime measured at 1000 cd/m^2.

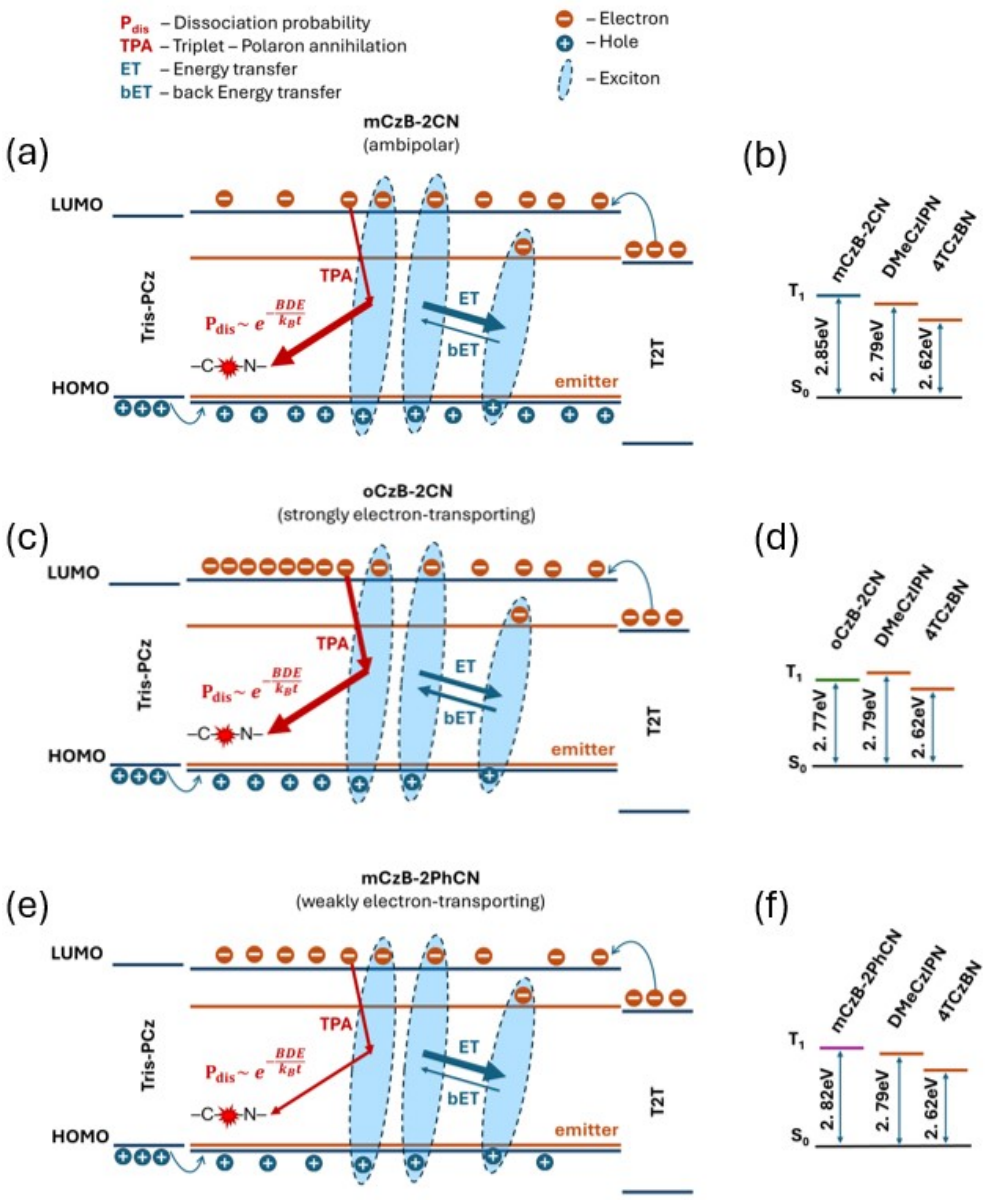

Figure S8. Schematic illustration of host–guest energy transfer and exciton–polaron interaction pathways in blue TADF-OLEDs employing the hosts **mCzB-2CN** (a,b), **oCzB-2CN** (c,d), and **mCzB-2PhCN** (e,f). Panels (a,c,e) depict exciton formation in the emissive layer, host-to-emitter energy transfer (ET), possible back energy transfer (bET), and triplet–polaron annihilation (TPA) as a representative exciton–polaron process linked to electrically induced bond scission. Arrow thickness qualitatively reflects the relative likelihood of each pathway among the hosts. Panels (b,d,f) compare the host and emitter triplet energy levels (T_1) to indicate triplet confinement and the probability for back transfer. Carrier symbols illustrate the different charge-transport tendencies of the hosts.

Table S3. Calculated bond dissociation energies (eV) for bonds 1–4 in carbazole–biphenyl hosts **mCzB-2CN**, **oCzB-2CN**, and **mCzB-2PhCN** in the neutral, anionic (–1), and cationic (+1) charge states. Bond indices correspond to the positions highlighted in the molecular structures on the right.

Molecule	Bond	Neutral	Anion (-1)	Cation (+1)
mCzB-2CN	1	6.06	3.34	6.82
	2 (C-N)	3.22	0.75	3.67
	3	5.01	4.52	6.06
	4	4.98	4.63	5.93
oCzB-2CN	1	4.59	3.88	5.52
	2	4.84	4.25	5.71
	3 (C-N)	3.22	0.73	3.45
	4	6.06	3.24	6.64
mCzB-2PhCN	1	4.97	31.54*	5.81
	2	5.01	4.99	6.00
	3 (C-N)	3.64	2.22	3.78
	4	5.91	3.62	6.46

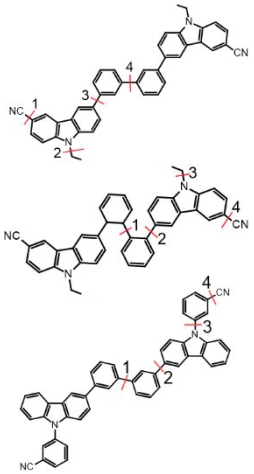

*Value did not converge

Table S4. Anionic-state C–N bond BDE of representative carbazole-phenyl-based hosts reported in the literature and in this work.

Host	BDE-1 (eV)	Reference
mCzB-2CN	0.75	This work
oCzB-2CN	0.73	This work
mCzB-2PhCN	2.22	This work
mCP	1.36	[2]
SiDBFCz	1.82	[2]
mCBP	1.82	[3]
mCBP-CN	2.82	[3]
DCDPA	1.49	[3]
TCTA	2.04	[4]
BCzPh	1.5	[4]
oCzBN	1.54	[5]
mCzBN	1.60	[5]
pCzBN	1.648	[5]
DCz-oTP	1.75	[6]
DOB-oTP	2.66	[6]

Copies of NMR, MS spectra

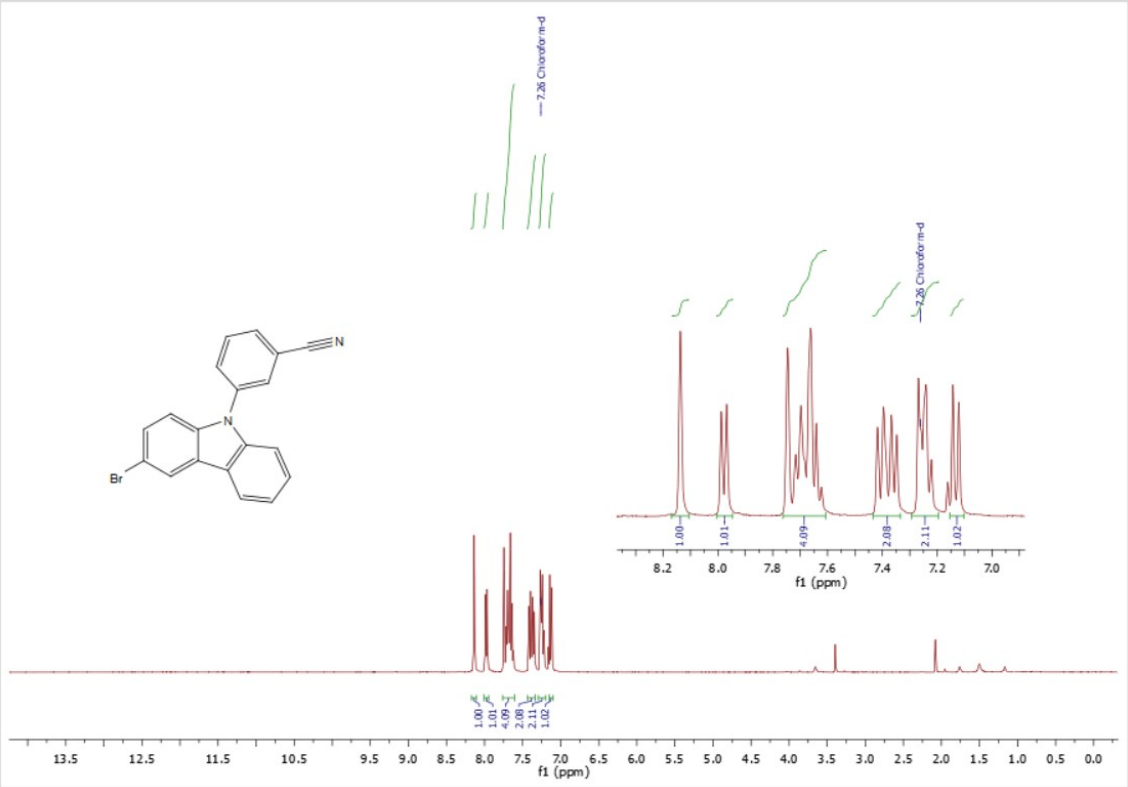

Figure S9. ^{1}H NMR of 3-(3-bromo-9H-carbazol-9-yl)benzonitrile

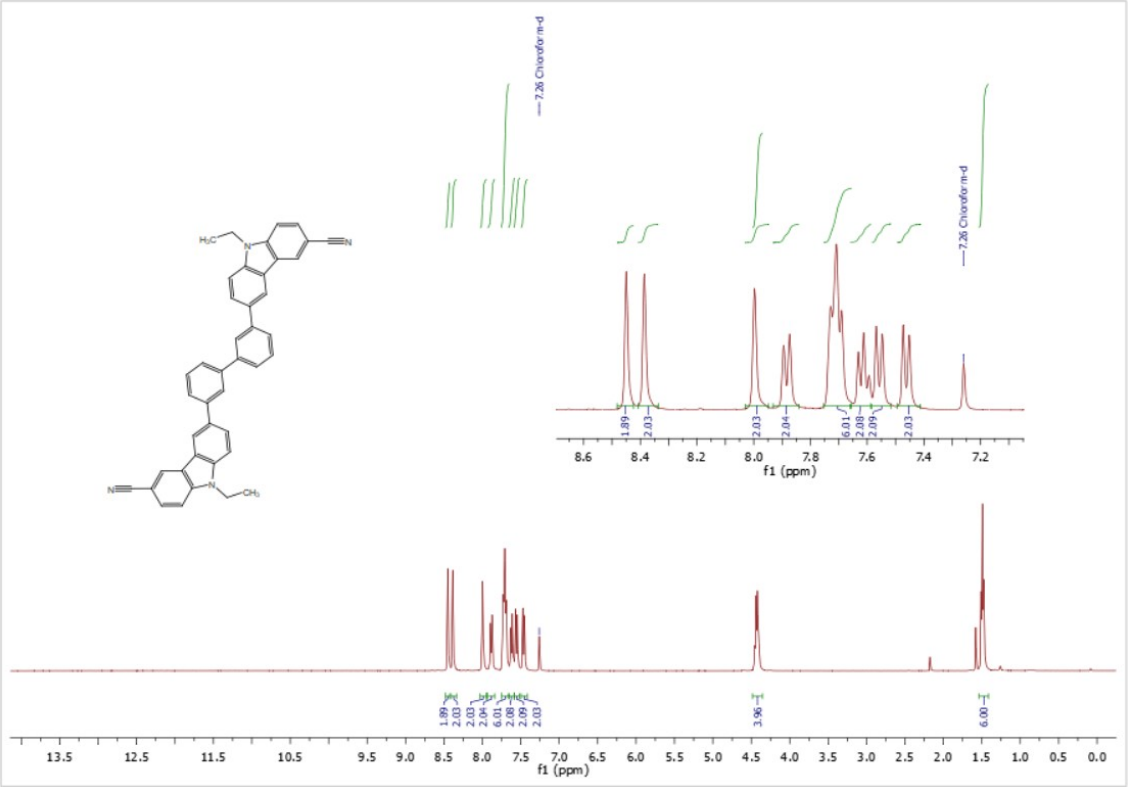

Figure S10. ^{1}H NMR of 6,6'-([1,1'-biphenyl]-3,3'-diyl)bis(9-ethyl-9H-carbazole-3-carbonitrile) (**mCzB-2CN**)

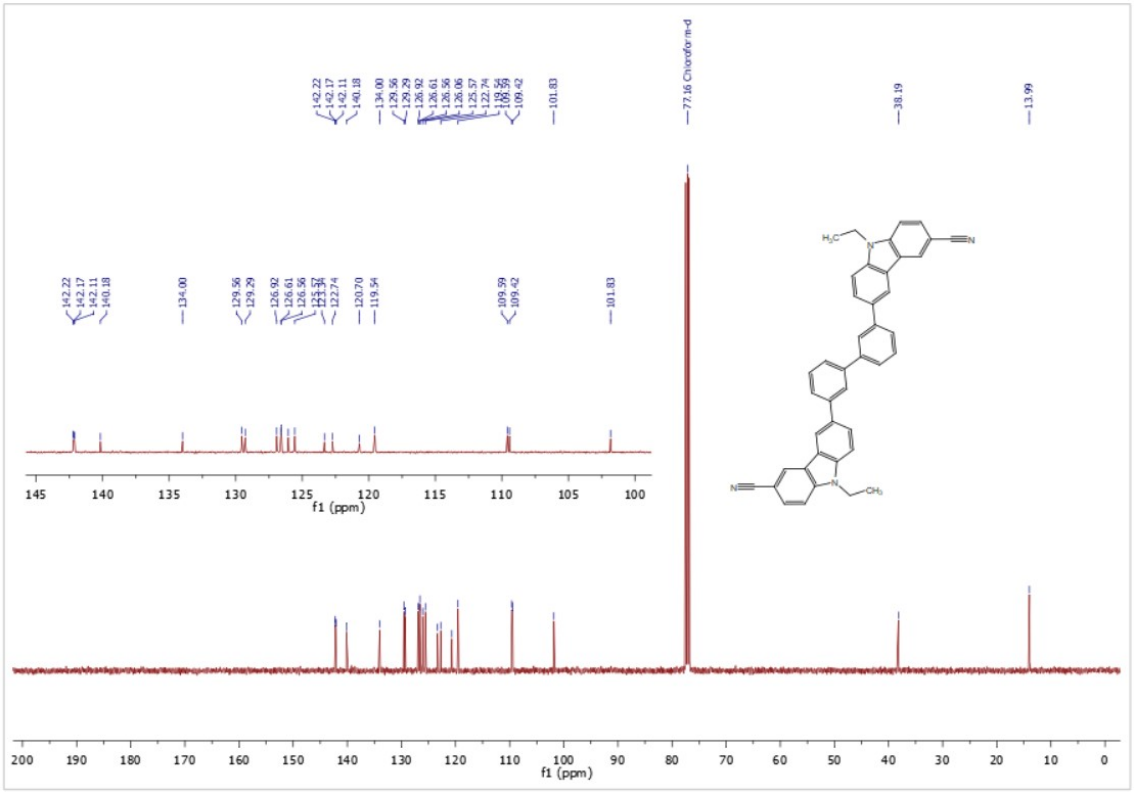

Figure S11. ^{13}C NMR of 6,6'-([1,1'-biphenyl]-3,3'-diyl)bis(9-ethyl-9H-carbazole-3-carbonitrile) (**mCzB-2CN**)

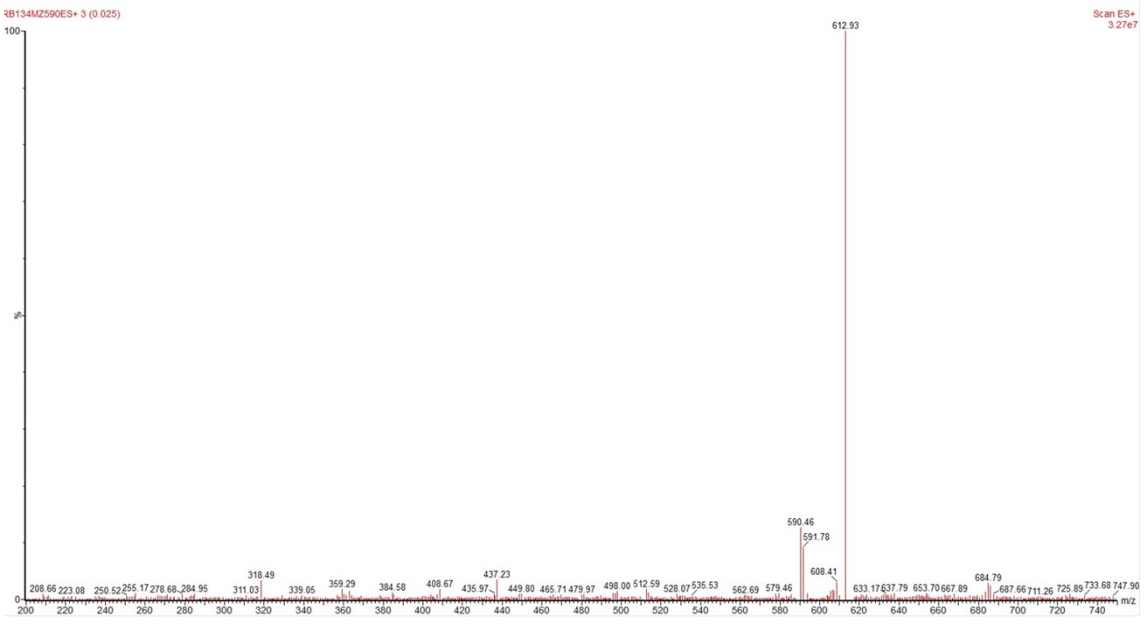

Figure S12. MS of 6,6'-([1,1'-biphenyl]-3,3'-diyl)bis(9-ethyl-9H-carbazole-3-carbonitrile) (**mCzB-2CN**)

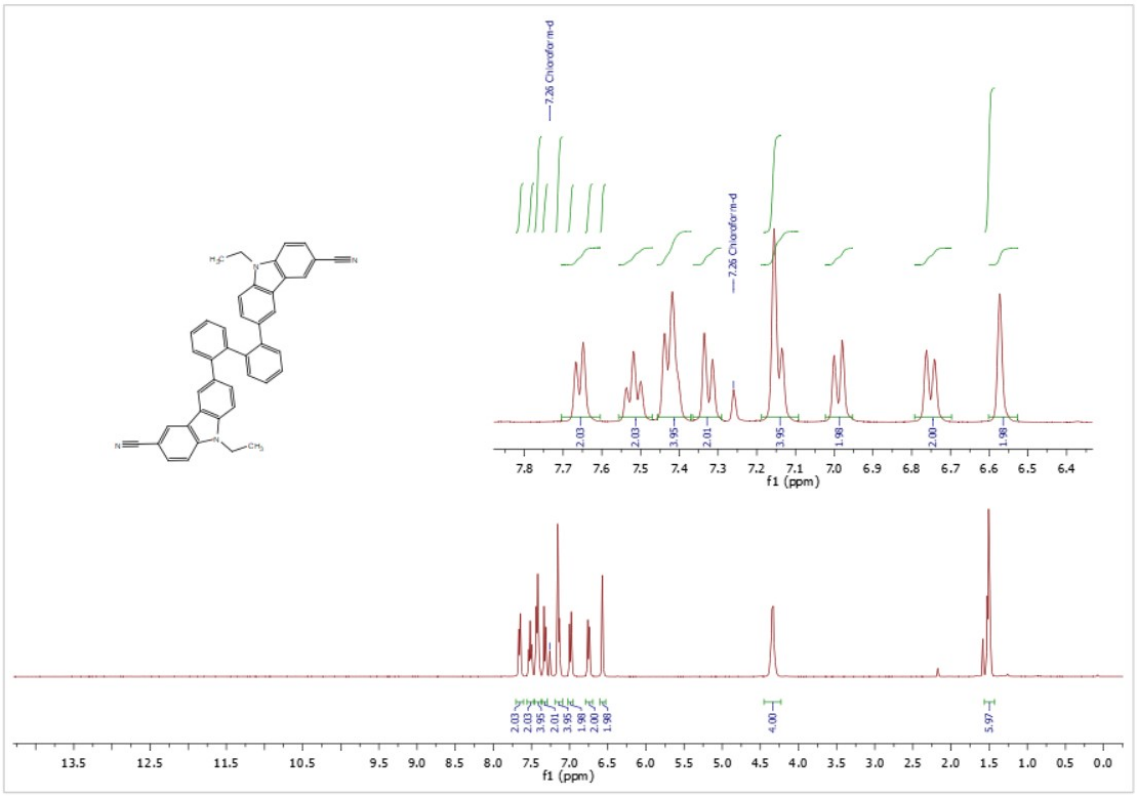

Figure S13. ^{1}H NMR of 6,6'-([1,1'-biphenyl]-2,2'-diyl)bis(9-ethyl-9H-carbazole-3-carbonitrile) (**oCzB-2CN**)

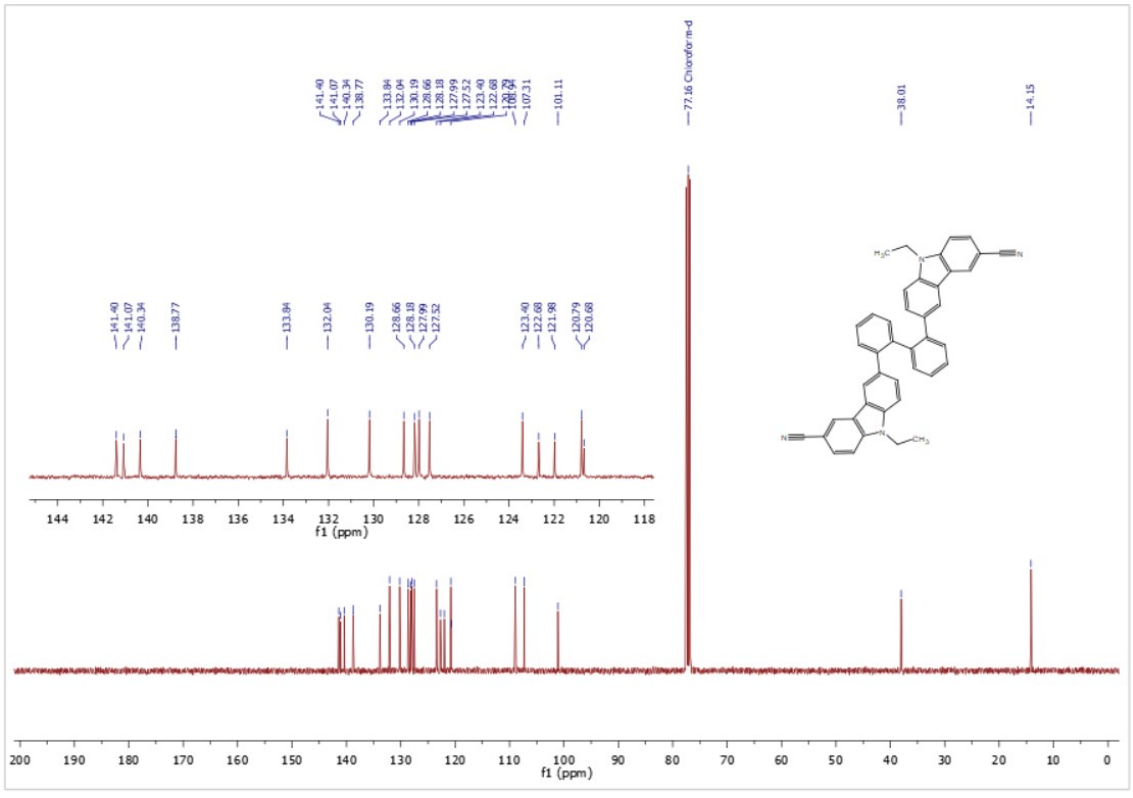

Figure S14. ^{13}C NMR of 6,6'-([1,1'-biphenyl]-2,2'-diyl)bis(9-ethyl-9H-carbazole-3-carbonitrile) (**oCzB-2CN**)

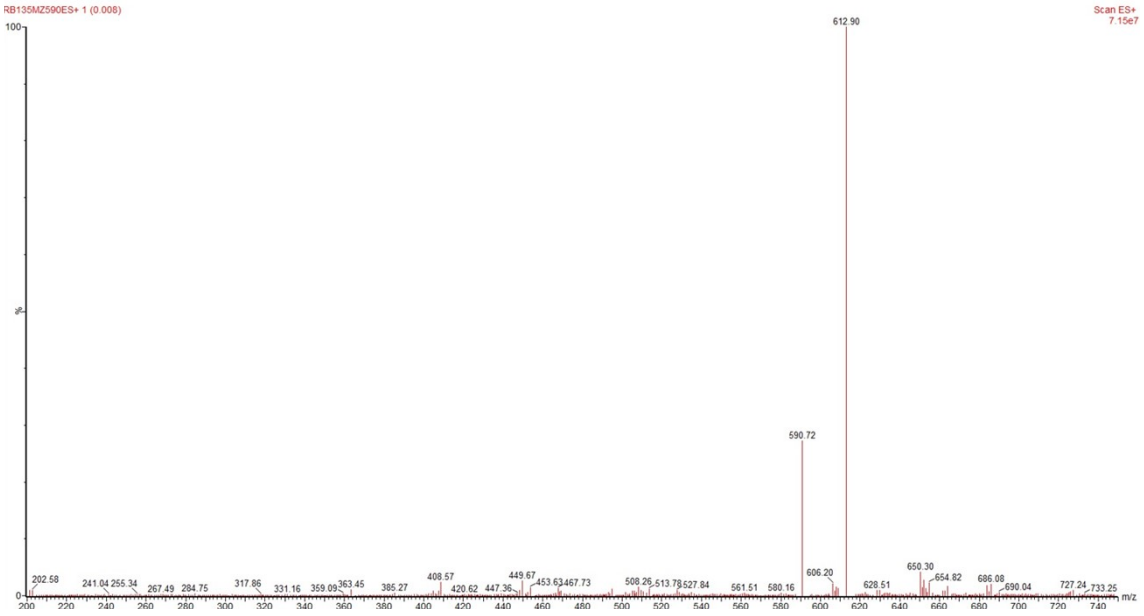

Figure S15. MS of 6,6'-([1,1'-biphenyl]-2,2'-diyl)bis(9-ethyl-9H-carbazole-3-carbonitrile) (**oCzB-2CN**)

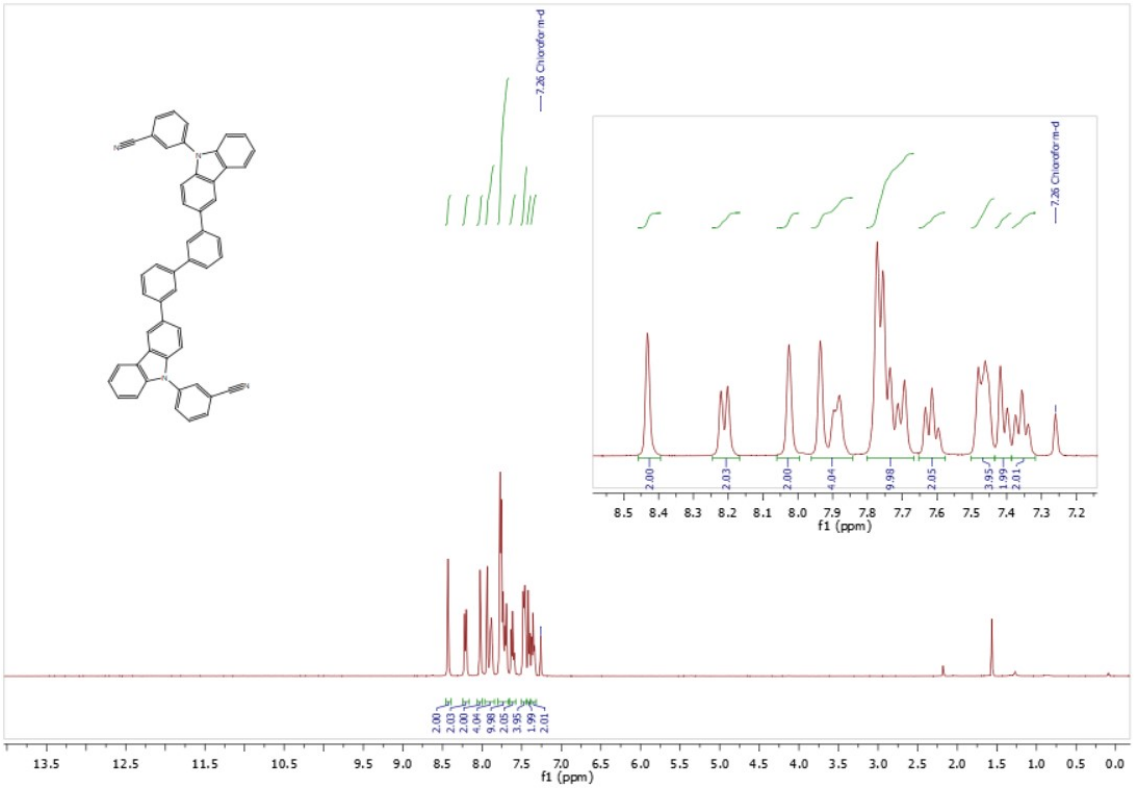

Figure S16. ^{1}H NMR of 3,3'-([1,1'-biphenyl]-3,3'-diylbis(9H-carbazole-3,9-diyl))dibenzonitrile (**mCzB-2PhCN**)

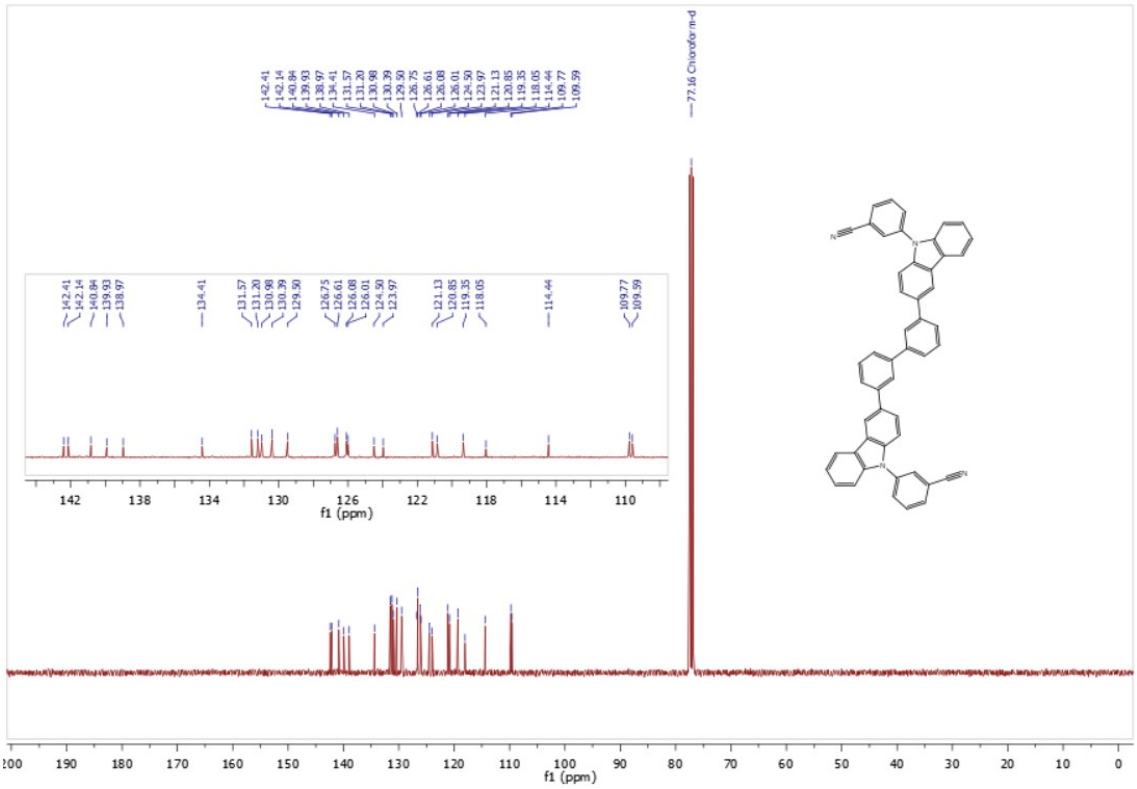

Figure S17. ^{13}C NMR of 3,3'-([1,1'-biphenyl]-3,3'-diylbis(9H-carbazole-3,9-diyl))dibenzonitrile (**mCzB-2PhCN**)

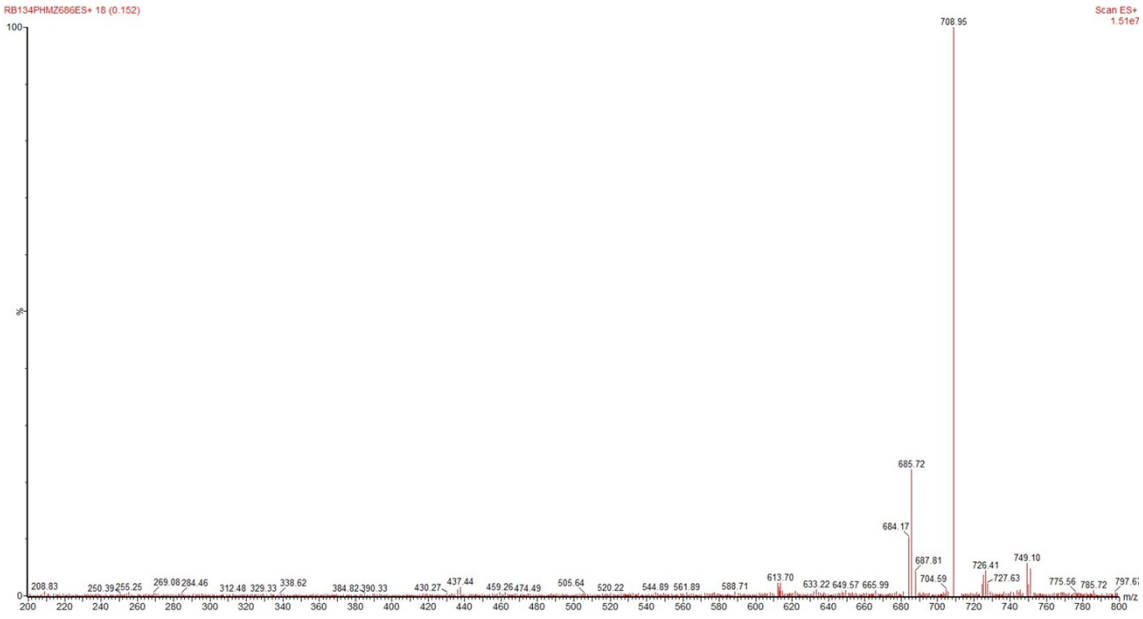

Figure S18. MS of 3,3'-([1,1'-biphenyl]-3,3'-diylbis(9H-carbazole-3,9-diyl))dibenzonitrile (**mCzB-2PhCN**)

References

1 A. Köhler and H. Bässler, *Electronic Processes in Organic Semiconductors: An Introduction*, Wiley-VCH Verlag GmbH & Co. KGaA, Weinheim, Germany, 2015.

2 S.-B. Ko, S. Kang and T. Kim, *Chem. Eur. J.*, 2020, **26**, 7767–7773.

3 D. H. Ahn, J. H. Maeng, H. Lee, H. Yoo, R. Lampande, J. Y. Lee and J. H. Kwon, *Adv. Optical Mater.*, 2020, **8**, 2000102.

4 Z. Wang, M. Li, L. Gan, X. Cai, B. Li, D. Chen and S.-J. Su, *Adv. Sci.*, 2019, **6**, 1802246.

5 C. Y. Yang, S. Kang, H. Jeong, H. J. Jang, Y. Lee and J. Y. Lee, *J. Mater. Chem. C*, 2020, **8**, 1697–1703.

6 T. H. Ha, S. W. Kang and C. W. Lee, *Org. Electron.*, 2024, **124**, 106960.